Semi-Automatic Tracking for Mitral Annulus Dynamic Analysis Using Real-Time 3D Echocardiography

F Veronesi[1,2], C Corsi[1], EG Caiani[2], L Sugeng[3], L Weinert[3],
V Mor-Avi[3], RM Lang[3], C Lamberti[1]

[1]Department of Electronics, Computer Science and Systems, University of Bologna, Italy
[2]Department of Bioengineering, Polytechnic of Milan, Italy
[3]University of Chicago Hospitals, Chicago, IL, USA

Abstract

Tissue Doppler is used to evaluate mitral annulus (MA) dynamics. This technique has two major limitations: it is two-dimensional and angle-dependent. To solve these limitations, our aim was to develop and test a tool for automated 3D tracking and quantification of the MA motion throughout the cardiac cycle by using real-time 3D echocardiography (RT3DE). The tracking algorithm was developed using a combination of two optical flow techniques in the 3D space. Transthoracic RT3DE imaging was performed in 45 subjects, including 15 normal subjects (NL) and 30 patients with mitral regurgitation (MR) due to dilated (n=15, DCM-MR) or ischemic (n=15, ISC-MR) cardiomyopathy. Our technique allowed the evaluation of MA geometry and the quantification of MA function parameters from RT3DE images, which were able to discriminate between NL, DCM-MR and ISC-MR subjects.

1. Introduction

Recent studies characterizing the mitral valve apparatus in both non-ischemic and ischemic cardiomyopathies have demonstrated geometric differences in mitral annular deformation with increased commissural-commissural as well as antero-posterior dimensions [1]. Similarly, differences in mitral annulus geometry have been described in anterior versus posterior myocardial infarction [2]. Observations in patients with dilated and ischemic mitral regurgitation (MR) have demonstrated that this is a disease of the remodelled myocardium instead of being secondary to an intrinsic valve disorder. In these patients, several studies have demonstrated that mitral regurgitation occurs in parallel with left ventricular (LV) remodelling.

However, little is known about the dynamic changes of the mitral valve annular surface area and annular longitudinal displacement throughout the cardiac cycle, since prior studies using real-time 3D echocardiography (RT3DE) have exclusively performed static measurements. We developed a tracking algorithm based on optical flow techniques to follow the position of the mitral annulus in 3D space throughout the cardiac cycle. Accordingly, our goal was to determine the dynamic changes of the mitral valve annulus surface area and longitudinal displacement throughout the cardiac cycle in normal subjects and in patients with mitral regurgitation (MR) secondary to dilated or ischemic cardiomyopathy using transthoracic RT3DE datasets.

2. Methods

2.1. Patient population

RT3DE datasets were acquired in 45 subjects (Philips Sonos 7500 scanner), including 15 normal subjects (10 males; age: 43±18 years) who were used as the control group and 30 patients divided into two groups. The first group included 15 patients with non-ischemic dilated cardiomyopathy (DCM-MR; 9 males; age: 51±10 years; end-diastolic volume: 291±126 ml; end-systolic volume 234±108 ml; ejection fraction 21±9%). Inclusion criteria were: 1) at least moderate mitral regurgitation with an effective regurgitant orifice area (EROA)≥0.2 cm²; 2) LV ejection fraction ≤30%; 3) normal arteries on coronary angiography. The second group included 15 patients with ischemic cardiomyopathy (ISC-MR; 9 males; age: 62±13 years; end-diastolic volume: 243±78 ml; end-systolic volume 178±76 ml; ejection fraction 25±7%). Inclusion criteria were: 1) the presence of moderate MR with an EROA $\geq$ 0.2 cm²; 2) at least double vessel coronary artery disease with lumen obstruction $\geq$ 50% on coronary angiography; 3) abnormal wall motion in ≥2 contiguous segments on 2D echocardiography.
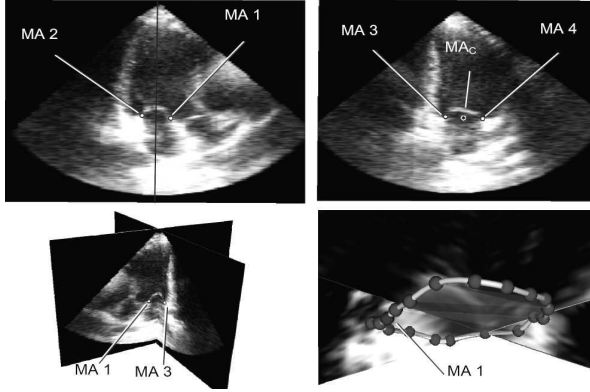
Figure 1. Manual initialization for the MA tracking procedure (see text for detail).

2.2. Mitral annulus initialization

The RT3DE datasets were analyzed to semi-automatically detect and track the mitral annulus throughout the cardiac cycle. Initially, a cut plane of the end-diastolic (ED) volume representing the 3-chamber view was manually selected. In this plane, two points were identified on the anterior (mitral annulus saddle-horn, MA1) and posterior (MA2) mitral valve annulus (figure 1, top left). This initialization was then repeated (MA3 and MA4, figure 1, top right) on an orthogonal plane crossing the center of the line connecting MA1 and MA2. The middle point of the segment connecting MA3 and MA4, was considered as the center of the mitral annulus (MA$_C$, figure 1, top right). Subsequently, ten long-axis cut planes evenly rotated around MA$_C$ (18° steps) were automatically displayed to complete the initialization procedure. On each of these planes, the operator manually selected two points, one on each side of the MA, and manually traced the mitral leaflets. Once this procedure was completed, the LV apex was manually selected.

Subsequently, the positions of each initialized MA point and the apex were automatically tracked frame-by-frame in 3D space throughout the cardiac cycle, using optical flow and region-based matching techniques performed with a likelihood function that is based on the assumption that both images are contaminated by a Rayleigh distributed multiplicative noise. Thereafter, the automatically tracked points were displayed in each frame to verify their position. Manual corrections were performed when required.

2.3. Mitral annulus tracking

The tracking of the initialized points was performed using a two-step optical flow technique. First, the Lucas-Kanade optical flow algorithm was applied. It is based on the assumption that the brightness $I(\mathbf{x},t)$ in the image is conserved during motion:

$$dI(\mathbf{x},t)/dt = 0.$$ (1)

In order to evaluate the velocity field $\mathbf{v}$ between two frames, a weighted least-square minimization of the following function is performed:

$$\sum_{\mathbf{x}\in\Omega} W^2(\mathbf{x})\left[\nabla I(\mathbf{x},t)\cdot\mathbf{v}+I_t(\mathbf{x},t)\right]^2$$ (2)

where the terms inside the square brackets are obtained by separating derivatives from (1), Ω is the domain containing the neighborhood of $\mathbf{x}$ (the initial point to be tracked) and $W(\mathbf{x})$ is a window, that gives more importance to central terms rather than for the ones in the periphery. The solution of the minimization of (2) is obtained by isolating $\mathbf{v}$ in matrix form:

$$\mathbf{v} = \left[A^T W^2 A\right]^{-1} A^T W^2 \mathbf{b},$$ (3)

where

$$A = \left[\nabla I(\mathbf{x}_1),...,\nabla I(\mathbf{x}_\lambda)\right]^T,$$
$$W = diag\left[W(\mathbf{x}_1),...,W(\mathbf{x}_\lambda)\right],$$
$$\mathbf{b} = -(I_t(\mathbf{x}_1),...,I_t(\mathbf{x}_\lambda))^T.$$

Once the velocity is known, the displacement of the point of interest is calculated as $\mathbf{d}_{LK} = \mathbf{v}\Delta t$, and the position of the point $\mathbf{x}$ in the next frame is given by :

$$\mathbf{x}_{LK} = \mathbf{x} + \left[\mathbf{d}_{LK}\right],$$ (4)

where square brackets mean rounding approximation.

As a second step, a block matching algorithm was applied, in order to evaluate the exact position of $\mathbf{x}$ into the next frame ($\mathbf{x}_{t+1}$). The matching was performed evaluating a maximum likelihood function based on the assumption that both images are contaminated by a Rayleigh distributed multiplicative noise. For each point inside a new 3D window $\mathbf{V}(\mathbf{x}_{LK})$ centered in $\mathbf{x}_{LK}$, another 3D window $\mathbf{F}(\mathbf{x})$ was defined and compared to the window of the same size around $\mathbf{x}$, by computing the likelihood estimator $E(\mathbf{x}_{t+1})$:

$$E(\mathbf{x}_{t+1}) =$$

$$\sum_{i=-m}^{m}\sum_{j=-m}^{m}\sum_{k=-m}^{m}\left\{\begin{array}{l}\ln(\mathbf{x}_t(i,j,k))\\-\ln(\mathbf{x}_{t+1}(i,j,k))\\-\ln(e^{2(\ln(\mathbf{x}_t(i,j,k))-\ln(\mathbf{x}_{t+1}(i,j,k))+1)})\end{array}\right\}$$ (5)

The maximum likelihood function was derived from Cohen and Dinstein work [3] considering that the noise in

two successive frame follows the same Rayleigh distribution.

The point corresponding to the maximum of $E(\mathbf{x}_{t+1})$ is the one that best fits the window around the starting point. The final point was then computed as:

$$\mathbf{x}_{t+1}^{final} = \arg\min E(\mathbf{x}_{LK}^{i}) \quad for \; \mathbf{x}_{LK}^{i} \in V(\mathbf{x}_{LK}) \quad (6)$$

Therefore, the final point was evaluated as the sum of the displacements computed from the two steps of tracking:

$$\mathbf{x}_{t+1}^{final} = \mathbf{x}_{LK} + \mathbf{d}_{M} = \mathbf{x}_{t} + \left[\mathbf{d}_{LK}\right] + \mathbf{d}_{M} , \qquad (7)$$

with $\mathbf{x}_{t}$ as the initial point at time t, $\left[\mathbf{d}_{LK}\right]$ as the rounded displacement evaluated by the Lucas-Kanade algorithm, and $\mathbf{d}_{M}$ as the displacement evaluated by the block matching technique.

The resulting point $\mathbf{x}_{t+1}^{final}$ was considered as the starting point for the tracking on the following frame. In this way the points selected by the operator were followed frame by frame throughout the cardiac cycle.

2.4. Mitral annulus measurements

From the MA surface tracked over the cardiac cycle, the following measurements were obtained and used to describe the dynamic behavior of the mitral annulus:
1) MA surface area (MASA) versus time. MASA changes were calculated for each consecutive frame as the difference between MASA and the area at end-diastole. Results were expressed as % of ED MASA. This parameter reflects the dynamic motion or pulsatility of the MA;
2) longitudinal displacement (in mm) of the MA throughout the cardiac cycle, computed as the average motion of all MA points along the long axis direction;
3) peak systolic (S'), early diastolic (E') and late diastolic (A') MA velocities, as the maximum absolute values during systole, early- and late-diastolic phases, respectively, of the MA velocity curve, computed as the first derivative of the MA displacement over time.

2.5. Statistical analysis

The computed parameters were averaged for all patients in each group. Data were presented as mean ± SD. Differences between the two cardiomyopathy subgroups versus normal group were tested using Kruskal-Wallis test, with Bonferroni correction for multiple comparisons. Differences between ISC-MR and DCM-MR group were tested using the rank-sum Mann-Whitney test. Differences were considered significant for p-values <0.05.

3. Results

Numerical results of measurements are showed in table 1. Significant inter-group differences were noted in ED MA surface area, which was larger in DCM-. The ED commissure-commissure and anterior-posterior annular diameters were significantly smaller in normal subjects (3.1 ± 0.4 cm and 2.4 ± 0.3 cm, respectively) compared to DCM-MR (3.8 ± 0.4 cm and 3.4 ± 0.5 cm and ISC-MR (3.5 ± 0.6 cm and 2.8 ± 0.4 cm), respectively (*p<0.05 versus normal). The maximum value of MA surface area occurred in correspondence with the rapid LV filling and was similar among groups. As a result, maximum MA surface area change showed statistically significant inter-group differences. Compared to normal subjects (56.4%), DCM-MR and ISC-MR groups had reduced MA surface area change (13.9% and 30.7% of MASA at ED, respectively).

When analyzing the MA surface area versus time curve in normal subjects, the maximal MA surface area occurred at 57.5% ± 3.2% of the RR interval (figure 2, bottom panel). In DCM-MR and ICM-MR, the largest MA surface area occurred significantly later in the cardiac cycle.

Longitudinal MA motion is shown in figure 2 (top). This plot depicted an initial downward deflection representing systolic motion of the MA towards the apex (figure 2, top panel). During the initial third of diastole, the MA moved towards the base corresponding to rapid LV filling. Subsequently, a period of minimal displacement was seen, followed by a rapid displacement corresponding to diastasis and atrial contraction. The maximum displacement from ED showed significant differences, both in magnitude and in timing (figure 2), with the normal group having larger and earlier MA
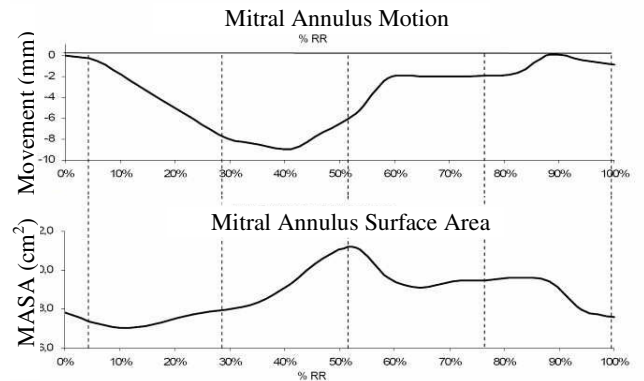

Figure 2. Graph depicting dynamic MA longitudinal motion (top panel) and MA surface area versus time plot (bottom panel). Both the curves were obtained in a normal subject. The MA motion versus time resembles LV volume versus time curve, whereas the MA surface area (MASA) resembles a left atrial volume versus time curve.

TABLE 1. Mitral annular parameters measured in the three study groups. MA= mitral annulus; Values expressed as mean ± SD; * Statistical difference versus normal (Kruskal-Wallis test, p<0.05); † Statistical difference versus ischemic (Mann-Whitney test; p<0.05).

	NL (n=15)	DCM-MR (n=15)	ISC-MR (n=15)
MA surface area ED, cm^2	6.9 ± 1.8	11.1 ± 2.6*†	9.0 ± 2.0*
Maximum MA surface area, cm^2	10.5 ± 2.0	12.6 ± 2.7	11.6 ± 2.6
Maximum MA surface area Change, %	56.4 ± 18.1	13.9 ±8.7*†	30.7 ± 12.7*
Maximum MA surface area timing, % of RR	57.5 ± 3.2	66.8 ± 7.1*	64.0 ± 7.5*
MA maximum displacement from ED, mm	-10.0 ± 3.0	-3.4 ± 1.7*†	-4,9 ± 1.5*
Maximum MA Displacement timing, % of RR	44.7 ± 6.2	56.5 ± 8.6*	52.8 ± 5.4*
MA Peak Systolic Velocity, mm/s	-39.3 ± 12.3	-18.9 ± 6.2*†	-24.0 ± 7.0*
MA Early Diastolic Velocity, mm/s	72.6 ± 31.5	23.0 ± 6.9*	30.9 ±16.2*
MA Late Diastolic Velocity, mm/s	26.5 ± 10.8	13.5 ± 9.1*	19.6 ± 11.2*

maximum displacement. S', E' and A' MA velocities were significantly lower in both DCM-MR and ISC-MR compared to normal subjects. Moreover, the DCM-MR group had lower peak systolic MA velocities and smaller maximum MA displacement compared to ISC-MR.

4.   Discussion and conclusions

Tissue Doppler imaging allows the evaluation of regional MA velocity. However, this method has two major limitations: 1) velocity measurements represent small regions of the MA, usually acquired from standard apical views and thus can be inaccurate; 2) measurements are dependent on the incidence angle of the acoustic beam. Consequently, the medial and lateral segment velocities cannot be accurately measured in the short axis view. The tracking technique used in this study allowed us to circumvent these limitations and quantify surface area, global longitudinal displacement and velocities of the MA on a frame-by-frame basis from RT3DE datasets.

We found that the MA displacement time curves resemble in their morphology the LV volume versus time. The magnitude of the MA longitudinal displacement has been shown to correlate with overall ventricular performance [4]. Not surprisingly, the annular displacement was largest in normal subjects, decreased in DCM-MR patients, whereas the values for ISC-MR were intermediate between these two groups. The time required to achieve peak longitudinal displacement was longer in both MR groups compared to normal subjects. Also, in these groups the longitudinal MA displacement was reduced, had lower velocities, and peak motion occurred later compared to normal subjects.

The methodology hereby described allows the computation of dynamic 3D changes that occur in MA surface and displacement throughout the cardiac cycle. This method can be used to better characterize the MA behaviour in pathologies such as DCM-MR or ISC-MR.

References

[1] Kwan J, Shiota T, Agler DA, Popovic ZB, Qin JX, Gillinov MA, Stewart WJ, Cosgrove DM, McCarthy PM, Thomas JD. Geometric differences of the mitral apparatus between ischemic and dilated cardiomyopathy with significant mitral regurgitation: real-time three-dimensional echocardiography study. Circulation. 2003;107(8):1135-40.

[2] Watanabe N, Ogasawara Y, Yamaura Y, Wada N, Kawamoto T, Toyota E, Akasaka T, Yoshida K. Mitral annulus flattens in ischemic mitral regurgitation: geometric differences between inferior and anterior myocardial infarction: a real-time 3-dimensional echocardiographic study. Circulation. 2005;112(9 Suppl):I458-I462.

[3] Cohen B, Dinstein I. New maximum likelihood motion estimation schemes for noisy ultrasound images. Pattern Recognition. 2002;35(2):455-63.

[4] Emilsson K, Alam M, Wandt B. The relation between mitral annulus motion and ejection fraction: a nonlinear function. *J Am Soc Echocardiogr*. 2000;13(10):896-901.

Address for correspondence

Federico Veronesi
DEIS, Viale Risorgimento 2, 40136 Bologna, Italy
federico.veronesi@polimi.it